Journal of Geosciences, Osaka City University
Vol. 33, Art. 2, p. 49-67
March, 1990

Nature of Lattice Microstrain of Microcrystalline Quartz and its Change in the Process of Grain Growth

Hiroyuki NAGAO*

(with 7 Figures, 4 Tables and 2 Plates)

Abstract

Chert and metachert whose grain size of quartz varies between 0.05 μm and 180 μm were investigated in terms of lattice microstrain of quartz, based on the experimental study of X-ray line broadening analysis and direct TEM observation of dislocations. Lattice microstrain obtained by X-ray line broadening analysis monotonously decreased as the grain size increases. On the other hand, microstrain due to dislocations first increased and then decreased with increasing grain size, having its largest value in the middle of the grain growth. A mechanism was proposed in order to explain rationally the change of the microstrain without taking tectonic stress during metamorphism into consideration, assuming that a large amount of hydroxyl impurities compensates lattice microstrain of microcrystalline quartz derived from surface tension. Dislocations observed in the middle stage of the grain growth was considered to be associated with the diffusion of excess impurities.

Introduction

Amorphous silica in soft siliceous sediments of off-shore environments changes into microcrystalline low-temperature quartz in the process of diagenesis via metastable opal of crystobalite structure. Further heating due to metamorphism causes grain growth of the microcrystalline quartz. Metamorphosed siliceous rocks, such as metachert or novaculite, often provide a number of valuable information about the metamorphism as their high quartz content makes analysis and interpretation easy and simple.

It has been demonstrated that the microcrystalline quartz in the siliceous rock, as well as fibrous quartz (chalcedony) in volcanic agate, has physical and chemical characteristics very different from those of ordinary quartz; for example, a high water content, a low refractive index and density, and broadening of the X-ray diffraction line profiles (FLÖRKE *et al.*, 1982; MIEHE *et al.*, 1984; GRAETSCH *et al.*, 1985, 1987; FRONDEL, 1982; MURATA and NORMAN, 1976). The role of silanole groups which is adsorbed on surfaces at open porosities and of hydroxyl impurities at twin-lamellae boundaries in chalcedony was recently demonstrated, although the water content of microcrystalline quartz has been interpreted as being due to the presence of water-containing amorphous opal or a large number of water-filled micropores (MIEHE *et al.*, 1984; GRAETSCH *et al.*, 1985, 1987).

* Central Research Laboratory, Nippon Sheet Glass Co. Ltd. Kaidosita, Konoike, Itami City, 664 JAPAN.

In fact, some macroscopic features of microcrystalline quartz, especially density and refractive indexes, seem to depend on the overall content of water, most of which is not structurally incorporated into quartz.

On the other hand, the origin of the X-ray line broadening or the quantitative analysis of lattice mocrostrain in microcrystalline quartz has not been investigated well. A recent X-ray line broadening study revealed that the lattice microstrain of microcrocrystalline quartz increases proportionally with the reciprocal of the crystallite size and it may be ascribed to the internal pressure derived from the surface tension (NAGAO and AIKAWA, 1988). It seems very interesting to investigate the lattice microstrain of quartz in the process of grain growth caused by metamorphism. In this study, chert and metachert whose grain size of quartz varies between 0.05 μm and 180 μm were investigated in terms of lattice microstrain of quartz, based on the experimental study of X-ray line broadening analysis and direct observation of dislocations.

Geologic setting of samples

The Ryoke metamorphic belt, which is paired with the high pressure type Sanbagawa metamorphic belt, is a typical low pressure type regional metamorphic belt in southwest Japan (MIYASHIRO, 1961). Pre-Cenozoic sedimentary strata of eugeosynclinal characters, which is mainly composed of mudstone, sandstone, chert, "greenstones", and limestone, are exposed over a wide area to the north of the Ryoke metamorphic belt. The southern parts of the sedimentary strata constitute low-grade zones of the Ryoke metamorphic belt. Discordant granitic intrusive bodies ubiquitously intruded into the strata and caused contact aureoles. Samples of Mesozoic chert and metachert were collected in three districts; they have been hardly metamorphosed in the Unuma distirct, metamorphosed by granitic rocks in the Kameoka district, and suffered to the Ryoke metamorphism in the Uji-Kasagi distirct (Fig. 1).

There is found Mesozoic bedded chert bearing well-preserved radiolarian remains in the Unuma district. SHIBATA and MIZUTANI (1980) proved the Rb-Sr isochron age and the K-Ar whole rock age match well with one another and they are also concordant with its biostratigraphic age within a reasonable time-span which is necessary for soft and unsolidified sediment to become chemically closed. It is supposed that the chert has never undergone thermal or tectonic disturbances during and after solidification. Two chert samples were collected and examined.

A small granodiorite body which intruded discordantly into the sedimentary strata caused a contact aureole in the Kameoka district, Kyoto Prefecture, where hornfels bearing metamorphic biotite and cordierite occurs (NAGAHARA, 1969). Five metachert samples were collected in the chlorite zone, where metamorphic biotite is not observed in pelitic rocks, and six in the chlorite-biotite zone, where both metamorphic chlorite and biotite occur in metapelites. Some of the samples which were collected about 7 km distant from the granodiorite body looked hardly metamorphosed. Geographic positions of the samples are shown in Fig. 2.

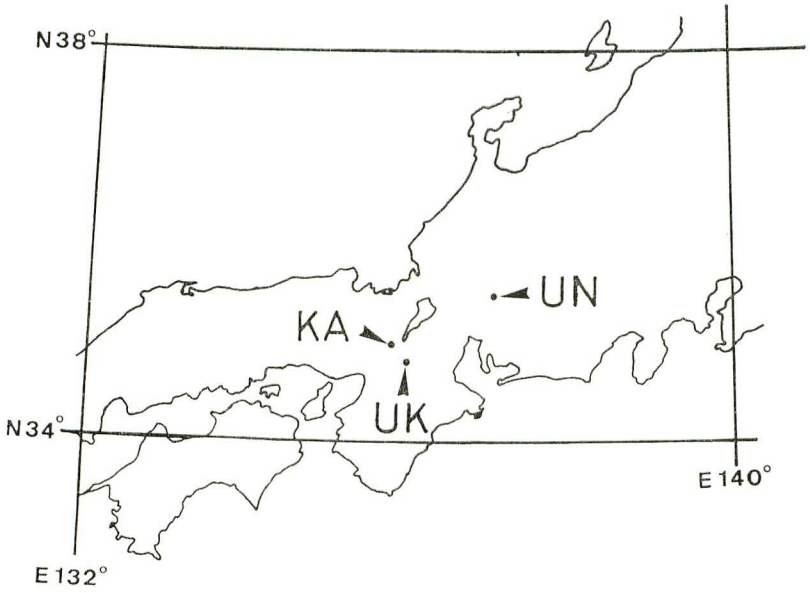

Fig. 1 Index map for studied districts. UN: Unuma district. KA: Kameoka district. UK: Uji-Kasagi district.

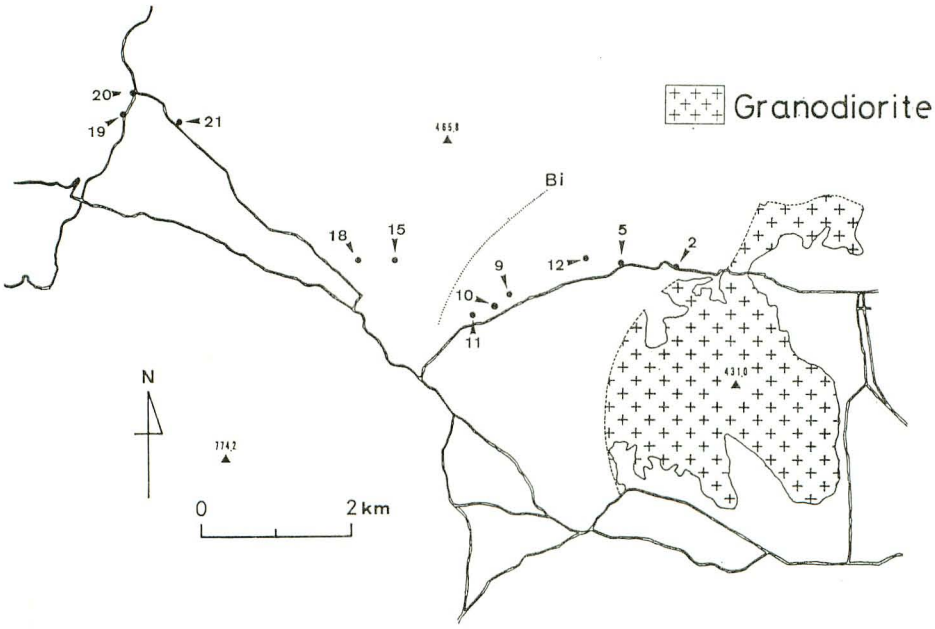

Fig. 2 Map for sampling localities in the Kameoka district. Bi: Biotite isograd.

The sedimentary strata in the Uji-Kasagi district, Kyoto Prefecture, were suffered to the Ryoke regional metamorphism and, in part, thermal metamorphism by granitic intrusive bodies (NAKAJIMA, 1960; HARA, 1962). Regional metamorphic grade largely increases from north to south and four mineral zones were defined on the basis of mineral paragenesis in pelitic rocks; namely chlorite, chlorite-biotite, biotite and sillimanite zones (WAN *et al.*, 1986). Seven metachert samples were collected in the chlorite zone, six in the chlorite-biotite zone, three in the biotite zone and one in the sillimanite zone. Geographic positions of the samples are shown in Fig. 3.

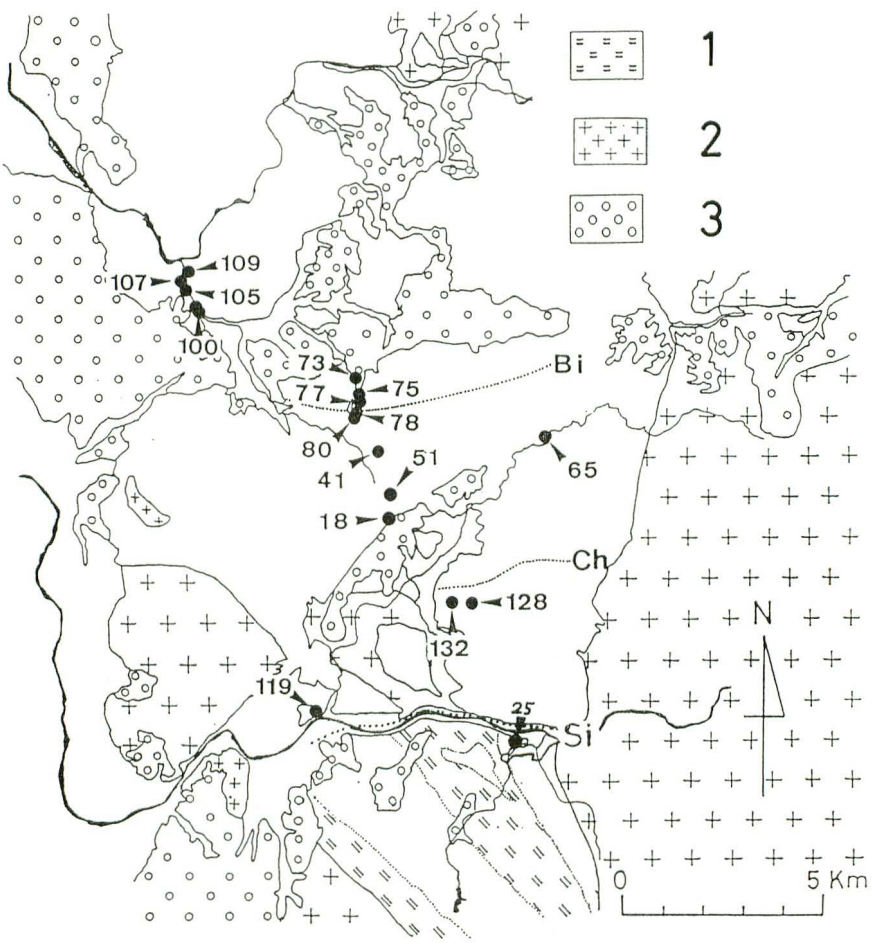

Fig. 3 Map for sampling localities in the Uji-Kasagi district. Bi, Ch and Si represent biotite, chlorite and sillimanite isograds, respectively. 1: Concordant granitic rocks. 2: Discordant granitic intrusive rocks. 3: Cenozoic sediments.

Experimental

(1) Grain size measurements

A geometric mean of the maximum and minimum diameters for every grain was measured with an optical microscope using a polished thin section. A mean of 50 grains was adopted as *grain size* for each sample. The section was made along a plane which is parallel to the principal mineral lineation and perpendicular to the principal planar structure in the case that such structures were recognized. The grain size was, however, determined with transmission electron microscopy or X-ray line broadening analysis when quartz grains were too small to be observed with optical microscopy.

(2) Transmission electron microscopy (TEM)

TEM was used to examine dislocation microstructures in quartz grains and, in some cases, to determine the grain size. Specimens thin enough for TEM study were prepared from 25 μm thin sections by ion-bombarment and examined in a HITACH HU-128E electron microscope, equipped with a tilting stage, operated at 100 kV. Dislocation density was determined by the number of dislocations intersecting a circle placed on the micrograph.

(3) X-ray diffraction analysis

The chert and metachert samples were crushed into powders with the range from 63 μm to 125 μm in diameter. By way of precaution the powders were purified in hot phosphoric acid for ten minutes to remove some non quartz impurities. They were then ground by an automatic agate-mortar for ten minutes and finer powders in the 5 μm to 20 μm range were obtained by means of sieving with 20 μm mesh sieves and precipitation in ethanol using the Stokes' formula. In practice grinding for more than an hour made X-ray diffraction line profiles a little broadened, however, this was not the case when grinding for less than half an hour. The pulverized samples ($5\sim20$ μm) were carefully mounted in a glass-holder and set in the powder diffractometer RIGAKU RAD-1A, operated at 45 kV 25 mA using copper K_α radiation with a nickel filter.

For X-ray line broadening analysis, diffraction profiles of the zoned reflection (namely $11\bar{2}0$, $22\bar{4}0$ and $33\bar{6}0$) were measured by the ω–2θ step scanning technique, typically every 0.002° (2θ) for $2\sim10$s. The integral breadth for each reflection was then calculated by a profile-fitting technique with the assumption that $K_{\alpha1}$ radiation is just twice intensity of $K_{\alpha2}$ radiation. The measured integral breadths were corrected for instrumental broadening to yield pure breadths assuming that both pure and instrumental profiles can be fitted to the modified Lorentzian shape. To measure the instrumental broadening, the author used the observed profile obtained from the pulverized specimen of an euhedral, colorless, and transparent Brazilian rock crystal. The specimen was prepared in the same procedure as already described and additionally dipped for an hour in a solution of 3 parts of 55% hydrofluoric acid in 97 parts of concentrated nitric acid so as to remove any very fine particles.

Calculation of lattice microstrain

(1) Lattice microstrain deduced by X-ray line broadening analysis

X-ray line broadening generally arises both from lattice parameter variation and from small size of X-ray coherent domains. The former strain broadening (β strain) and the latter size broadening (β size) are expressed by the equations,

$$\beta \text{ strain} = 4\varepsilon \tan\theta \qquad (1)$$

$$\beta \text{ size} = K\lambda/D\cos\theta \qquad (2)$$

where ε is mean lattice microstrain, D is a mean crystallite size, λ is the X-ray wavelength, K is a constant near unity and θ is the Bragg angle (*e.g.* KLUG and ALEXANDER, 1954).

The sample broadening, after instrumental correction, should be divided into the two components. The two types of broadening represent different dependency on the diffraction angle, as is shown in equations (1) and (2). Thus, in principle, these two components can be evaluated using at least two sample breadths of parallel planes ($hh\bar{2}h0$, as an example), which should give the same lattice strain and crystallite size. This is the so-called WARREN & AVERBACH method in the real space (*e.g.* WARREN, 1959). Breadth relation which was used in order to convolute the two types of broadening had been obtained by SHOENING (1965):

$$\beta \text{ sample} = (2\beta \text{ strain} + \beta \text{ size})^2/(4\beta \text{ strain} + \beta \text{ size}) \qquad (3)$$

Hereafter, the lattice strain obtained by the X-ray line broadening analysis is designated as *X-ray microstrain*. The analytical details of the X-ray analysis are to be published in NAGAO and AIKAWA (1985).

(2) Determination of lattice microstrain due to dislocations

Lattice distortion around dislocations is one of the major causes of X-ray line broadening. The magnitude of microstrain due to dislocations was quantitatively calculated in order to compare the X-ray microstrain with the dislocation density measured directly with TEM. This microstrain is, hereafter, designated as *dislocation microstrain*.

The general relation of lattice microstrain and the density of dislocations was derived by HORDON and AVERBACH (1961). Assuming that dislocations are distributed randomly and homogeneously and that half the dislocations are edges and screws, then the mean square strain (ε_{ms}) acting normal to the diffraction plane was given by

$$\varepsilon_{ms} = \frac{2\rho b^2}{\pi^2}\ln\left(\frac{1}{4b\sqrt{\rho}}\right)\left[\frac{8A^2+4AB+B^2}{8}\cos^2\Delta + \frac{8A^2-4AB+B^2}{8}\cos^2\Psi + \frac{1}{4\pi}\sin^2\Psi\right] \qquad (4)$$

$$A = [4(1+\nu)]^{-1}$$

$$B = [2(1-\nu)]^{-1}$$

where b is the length of Berger's vector (**b**), ν is Poisson's ratio, Δ is the angle between

the diffraction plane normal (**N**) and the dislocation glide plane normal, Ψ is the angle between **N** and **b**, and ρ is the density of dislocations.

Considering all dislocations are the basal slip in the **a** directions, the easiest slip system in quartz (NICHOLAS and POIERIE, 1976), then the mean square strain for hh$\bar{2}$h0 X-ray reflections is given by

$$\varepsilon_{ms} = 2.61 \times 10^{-17} \rho \ln (5.1 \times 10^{6} \rho^{-0.5}) \quad (5)$$

For a Gaussian strain distribution ε_{ms} is given by

$$\varepsilon_{ms} = 0.64 \varepsilon_{d}^{2} \quad (6)$$

where ε_d is the dislocation microstrain which corrsponds to the integral breadth. Hence, the relation between dislocation microstrain and the density of dislocations for quartz was given from equations (5) and (6):

$$\varepsilon_{d}^{2} = 4.08 \times 10^{-17} \rho \ln (5.1 \times 10^{6} \rho^{-0.5}) \quad (7)$$

Results

X-ray diffraction analysis showed that all of the samples consisted of low-temperature quartz with a small amount of phylosilicates. The grain size and the X-ray microstrain for each sample are listed in Tables 1～3. TEM observation was done for five of the samples. The dislocation density and the dislocation microstrain are listed in Table 4.

(1) Hardly metamorphosed chert in the Unuma district

X-ray line broadening was so severe that the 33$\bar{6}$0 reflection was not measured. The

Table 1 Grain size and X-ray microstrain of hardly metamorphosed chert in the Unuma district.

Sample	X-ray microstrain	Grain size
UN01	9.7×10^{-4}	95(nm)
UN02	1.1×10^{-3}	53

Table 2 Grain size and X-ray microstrain of metachert of the contact aureole in the Kameoka district.

Sample	Minral zone	X-ray microstrain	Grain size
KA2	chl-bio	3.2×10^{-4}	28(μm)
KA5	chl-bio	3.7×10^{-4}	14
KA9	chl-bio	4.3×10^{-4}	10
KA10	chl-bio	6.4×10^{-4}	7.7
KA11	chl-bio	5.3×10^{-4}	8.2
KA12	chl-bio	3.8×10^{-4}	6.2
KA15	chlorite	3.8×10^{-4}	5.8
KA18	chlorite	5.8×10^{-4}	6.3
KA19	chlorite	5.2×10^{-4}	0.4
KA20	chlorite	5.0×10^{-4}	0.4
KA21	chlorite	5.2×10^{-4}	0.6

Table 3 Grain size and X-ray microstrain of metachert of the Ryoke metamorphic belt in the Uji-Kasagi district.

Sample	Minral zone	X-ray microstrain	Grain size
UK25	sillimanite	0.8×10^{-4}	180(μm)
UK119	biotite	3.1×10^{-4}	44
UK128	biotite	1.8×10^{-4}	51
UK132	biotite	2.6×10^{-4}	48
UK18	chl-bio	2.7×10^{-4}	22
UK41	chl-bio	5.0×10^{-4}	10
UK51	chl-bio	3.4×10^{-4}	21
UK65	chl-bio	3.1×10^{-4}	22
UK78	chl-bio	4.2×10^{-4}	6.1
UK80	chl-bio	4.7×10^{-4}	8.2
UK73	chlorite	6.0×10^{-4}	6.7
UK75	chlorite	6.8×10^{-4}	5.4
UK77	chlorite	6.1×10^{-4}	5.4
UK100	chlorite	5.9×10^{-4}	6.2
UK105	chlorite	5.5×10^{-4}	5.4
UK107	chlorite	7.0×10^{-4}	5.8
UK109	chlorite	5.7×10^{-4}	6.8

Table 4 Dislocation density and the dislocation microstrain of some chert samples.

Sample	Dislocation density	Dislocation microstrain
UN01	$<1\times10^{8}/cm^{2}$	$<1.6\times10^{-4}$
KA21	$1\times10^{8}/cm^{2}$	1.6×10^{-4}
KA15	$5\times10^{8}/cm^{2}$	3.3×10^{-4}
UK41	$1\times10^{9}/cm^{2}$	4.6×10^{-4}
UK128	$3\times10^{7}/cm^{2}$	9.1×10^{-5}

X-ray line broadening analysis indicated that the grain size was $50\sim100$ nm and the X-ray microstrain was about 1.0×10^{-3}. One of the samples were examined with TEM (Plate 1, Fig. 1). It showed quartz grains of about 100 nm in diameter. The grains were largely bordered by curved grain boundaries. Dislocations were hardly observed and their density was estimated less than $1\times10^{8}/cm^{2}$.

(2) Metachert in the Kameoka district

The grain size of quartz, which generally decreased with the distance from the granodiorite body, varied $0.5\sim10$ μm in the chlorite zone and $10\sim30$ μm in the chlorite-biotite zone. On the other hand, the X-ray microstrain, which varied between 3×10^{-4} and 7×10^{-4}, decreased subtlely as the distance decreases (Fig. 4).

Two of the metachert, whose grain sizes were 0.6 μm and 5.8 μm, in the chlorite zone were examined with TEM. The former metachert mainly consisted of equant and polygonal quartz grains (Plate 1, Figs. 2–3). Three grain boundaries often intersected at far different angles from 120°. Grain boundaries were generally curved to a small extent. Images of small dislocation loops, which were sometimes arranged in line, were ubiquitonously observed in the quartz grains. The density of tangled dislocations was about $1\times10^{8}/cm^{2}$. On the other hand, the latter metachert generally had straight grain boundaries (Plate 1, Fig. 4). Three boundaries usually intersected at about 120°. A large

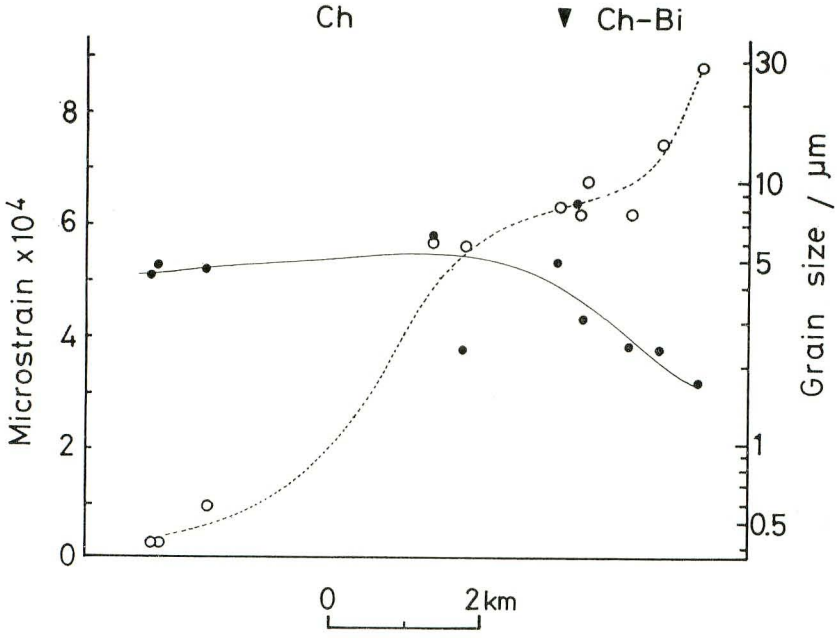

Fig. 4 Grain size and X-ray microstrain of quartz in the Kameoka district as a function of the distance from the granodiorite body. Open and solid circles represent grain size and X-ray microstrain, respectively. Ch: Chlorite zone. Ch-Bi: Chlorite-biotite zone.

number of tangled dislocations as well as dislocation loops were recognized in the quartz grains. The density of tangled dislocations was estimated about $5\times10^8/cm^2$.

(3) Metachert in the Ryoke metamorphic belt

Quartz grains were generally equant and polygonal. Textures suggestive of secondary recrystallization were partly recognized in some of the samples of higher grade zones. The grain size of quartz, which generally increased with metamorphic grade, varied $5\sim7$ μm, $6\sim22$ μm, $44\sim51$ μm and 180 μm in the chlorite, chlorite-biotite, biotite and sillimanite zones, respectively. In contrast, the X-ray microstrain abruptly decreased in the chlorite-biotite zone (Fig. 5).

Two of the metachert, whose grain sizes were 10 μm and 51 μm, were examined with TEM. The former metachert showed a large number of tangled dislocations, which usually connected small dislocation loops, in the quartz grains (Plate 2, Figs. 1–2). The density of tangled dislocations reached up to $1\times10^9/cm^2$. Lens-like voids were often recognized along grain boundaries (Plate 2, Fig. 3). On the other hand, tangled dislocations were hardly observed in the latter metachert (Plate 2, Fig. 4). Only a small number of dislocation loops were recognized in the quartz grains. The dislocation density was about $3\times10^7/cm^2$.

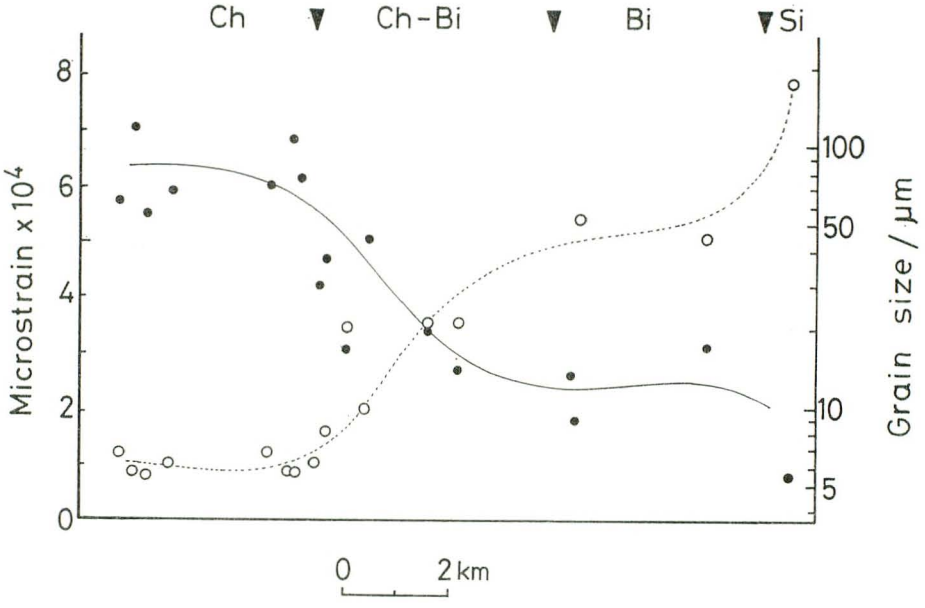

Fig. 5 Grain size and X-ray microstrain of quartz in the Uji-Kawasagi district with respect to metamorphic grades. Open and solid circles represent grain size and X-ray microstrain, respectively. Ch: Chlorite zone. Ch-Bi: Chlorite-biotite zone. Bi: Biotite zone. Si: Sillimanite zone.

Discussion

(1) Lattice microstrain of microcrystalline quartz

It should be noted that the hardly metamorphosed chert in the Unuma district ($0.05 \sim 0.1\ \mu$m in grain size) showed surprisingly large magnitudes of the X-ray microstrain. To give an example, lattice microstrain of 1×10^{-3} would be compatible with the dislocation density of some $1 \times 10^{10}/\text{cm}^2$ if it originated from dislocations in quartz grains. The author ascribes the large microstrain as being intrinsic to small crsystallites in cohesive microcrystalline aggregates.

As is well known, curved grain boundaries cause internal pressure. For example, a fine spherical crystallite of diameter D and surface energy γ has an internal pressure equal to $4\gamma/\text{D}$ (KINGERY, 1960). This should lead to lattice microstrain ($|\varepsilon|$) of small crystallite given by

$$|\varepsilon| \equiv \frac{\delta a}{a} = \frac{4\gamma}{3\kappa D} \qquad (8)$$

were κ is the bulk modulus of the crystallite (VERMAAK *et al.*, 1968; MAYS *et al.*, 1968). The constriction of the lattice spacing due to surface energy were already reported in the field of thin films and ultra-fine particles (VOOK and OTOONI, 1968; VERMAAK and

KUHLMANN-WILSDORF, 1968; WASSERMAN and VERMAAK, 1970). For instance, a vacuum evaporated thin gold film of several hundred angstroms in thickness has about 0.1% smaller lattice spacing than bulk gold. However, this phenomenon may not be directly related to the cohesive microcrystalline aggregate.

If you consider a two dimensional example of a cohesive polycrystalline aggregate where all grain boundaries are equal in energy and they meet to form angles of 120°, then all grains should have curved boundaries except six-sided grains (COBLE and BURKE, 1963). The curved boundary causes the internal pressure which makes the neighboring crystallites more or less distorted. The resultant lattice microstrain of each crystallite bordering the curved boundary has a different sign, namely, the strain is compressional for the crystallite having convex boundary when observed outward from the center of the crystallite and tensional for the crystallite having concave boundary. It is therefore obvious that, when you deal with a three dimensional cohesive microcrystalline aggregate consisting of only one phase, the observed lattice microstrain due to the surface energy does not result in a peak shift for the X-ray diffraction line profile but in its broadening. Moreover, the resultant lattice microstrain deduced from X-ray line broadening should be inversely proportional to the crystallite size.

In order to find the theoretical relationship between lattice microstrain and crystallite size calculated from equation (8), I shall adopt the bulk modulus (κ) and surface energy (γ) of quartz experimentally determined. Unit cell parameters used were those determined by a single crystal X-ray method and the bulk modulus of 0.38×10^{11} N/m^2 was obtained from the change of lattice parameters under several pressures (LEVIEN *et al.*, 1980). The surface energy of quartz was estimated to be about 5×10^{-1}J/m^2 for wet and/or hydrated surface and 20×10^{-1}J/m^2 for dry and/or fresh surface (PARKS, 1984). The surface energy for the $\{11\bar{2}0\}$ planes of natural quartz has been directly measured by cleaving a single crystal to be 7.6×10^{-1}J/m^2 (BRACE and WALSH, 1962). Assuming that the surface energy of natural quartz ranges from 5 to 20×10^{-1}J/m^2, then you can calculate the lattice microstrain ($|\varepsilon|$) of quartz microcrystallite by

$$|\varepsilon| = 1.8\sim7.2\times10^{-9}/D \qquad (9)$$

where D is a crystallite diameter in centimeters. The shaded area between the two dashed lines (upper; 20×10^{-1}J/m^2, lower; 5×10^{-1}J/m^2) in Fig. 6 displays the relationship between lattice microstrain and crystallite size given by equation (9). The plots obtained experimentally for some natural microcrystalline quartz (solid circles in Fig. 6) are in good agreement with the calculated ones in spite of some ambiguities in the calculation (NAGAO and AIKAWA, 1988).

Thus it may be concluded that the observed large lattice microstrain of quartz microcrystallites, as deduced from X-ray line broadening analysis to be inversely proportional to the crystallite size, is caused by the internal pressure derived from surface energy. The author also suspects that the peculiar physical and chemical characteritsics of the small

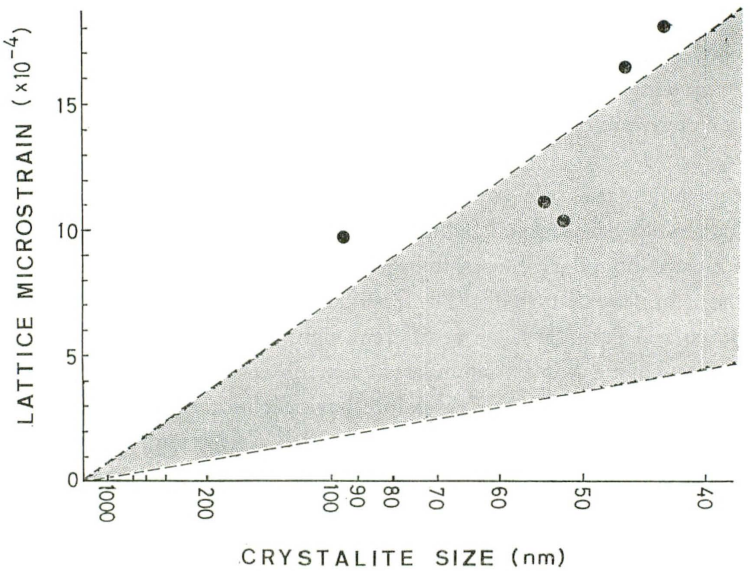

Fig. 6 Relationship between the X-ray microstrain and the reciprocal of the crystallite size. Solid circles represent the experimental values of natural microcrystalline quartz. Shaded area represents theoretical relation. After NAGAO and AIKAWA (1988).

crystallites in microcrystalline quartz aggregate should be ascribed to the large microstrain due to the inherent surface energy for microcrystalline aggregate.

(2) Lattice microstrain in the process of grain growth

Two kinds of lattice microstrain, the X-ray microstrain and the dislocation microstrain, were plotted in Fig. 7 as a function of the grain size of quartz. It clearly shows that the X-ray microstrain generally decreases with the increase of the grain size. On the other hand, the dislocation microstrain first increases and then decreases as the grain size increases, having its largest value in the middle of the grain growth. In order to make further discussion convenient and simple, the author tentatively divided the continuous process of the grain growth into three stages, as is shown in Fig. 7. The first, second and third stages roughly corrsepond to $0.05 \sim 0.5$ μm, $0.5 \sim 10$ μm and $10 \sim 180$ μm in quartz grain size, respectively.

In the first stage, the X-ray microstrain decreases rapidly and monotonously with increasing grain size, whereas the dislocation microstrain is negligibly small. This means that the X-ray microstrain is not caused by dislocations. A large extent of lattice distortion has been reported qualitatively for microcrystalline quartz (NORMAN and MURATA, 1976; GRAETSCH *et al.*, 1987). In the previous section, the author demonstrated that the large microstrain, as deduced from X-ray line broadening analysis to be inversely proportional to the crystallite size, might be intrinsic to small crystallites in cohesive aggregates and be caused by the internal pressure derived from surface tension. The rapid and

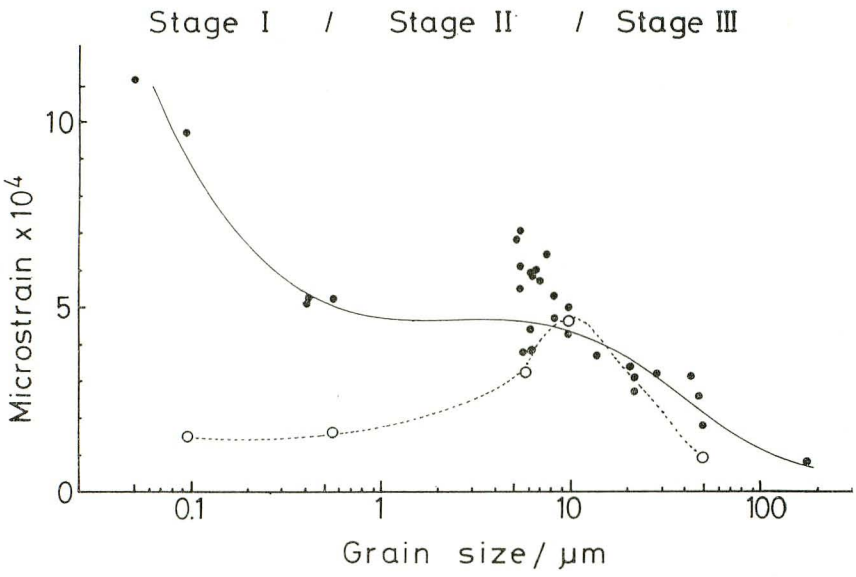

Fig. 7 X-ray microstrain and the dislocation microstrain as a function of the grain size. Solid and open circles represent X-ray and dislocation microstrain, respectively.

monotonous decrease of the X-ray microstrain, shown in Fig. 7, suggests that the X-ray microstrain in the first stage is caused by the internal pressure derived from surface tension.

In the second stage, the dislocation microstrain increases with increasing grain size, whereas the X-ray microstrain does not practically change. This means that the dislocation density increased while the grain size of quartz grains increases from 0.5 μm to 10 μm. It is difficult to deny the possibility that the dislocations originated from tectonic stress during the metamorphism. However, the possibility seems to be nominal as the increase of the dislocation microstrain was observed not only in the Ryoke metamorphic belt but also in the contact aureole.

The origin of the dislocations might be interpretable without taking the geologic stress into consideration (NAGAO and AIKAWA, in preparation). It seems rational to assume that hydroxyl groups compensate for lattice microstrain of microcrystalline quartz due to surface tension. This may be reasonable in energetics considering even a small amount of hydroxyl impurities reduces the elastic strength of quartz (GRIGGS, 1967). This assumption results in another presumption that the amount of hydroxyl groups incorporated within the crystal structure depends on the grain size of microcrystalline quartz. FRONDEL (1982) showed that microcrystalline chalcedonic quartz contains hydroxyls in structural sites and should be mineralogically distinguished from ordinary quartz.

If the hydroxyl content depends on the grain size, then hydroxyl groups should be diffused out of quartz grains while the grain size increases. The diffusion should continue

until all of the hydroxyl groups have been removed out of the grains. MCLAREN *et al.* (1983) investigated the process of hydroxyl diffusion in heat-treated synthetic quartz crystals. A large number of dislocation loops connecting water-bubbles were observed after heating the crystals. With increasing heating time, the dislocation loops gradually developed in size and finally became tangled with others. The generation and development of dislocations and water-bubbles were also reported by CORDIER and DOUKHAN (1989) for the precipitation of supersaturated water in quartz. These observations suggest that the hydroxyl impurities in quartz diffuse through dislocations, a high-diffusivity path for diffusion. The tangled dislocations and the dislocation loops in the metachert samples, as were described in the previous section, might be associated with the hydroxyl diffusion during the grain growth.

In the third stage of the grain growth, both the X-ray microstrain and the dislocation microstrain gradually decrease as the grain size increases. The two kinds of microstrain are consistent with each other, suggesting that dislocations in quartz are the main cause of the X-ray microstrain. Such a phenomena like this is usually observed when a crystal of high dislocation density is statically annealed at high temperatures.

Fig. 7 also suggests that extended heating of the metachert would result in normal grain growth in the usual sense, the statistical growth of strain-free quartz grains.

Acknowledgment

The author wishes to thank Dr. Nobuyuki AIKAWA for valuable discussions and constructive criticisms. Transmission electron microscopy was assisted by Dr. Kohji NOBUGAI of Osaka University to whom the author is indebted.

References

BRACE, W.F. and WALSH, J.B. (1962): Some direct measurements of the surface energy of quartz and orthoclase, *Am. Mineral.*, **47**, p. 1111–1122.

BURSILL, L.A. and MCLAREN, A.C. (1965): Transmission electron microscope observation of fracture in quartz and zircon, *J. Appl. Phys.*, **36**, p. 2084–2085.

COBLE, R.L. and BURKE, J.E. (1963): Sintering in ceramics, In BURKE, J.E. (ed) *Progress in Ceramic Science*, **3**, p. 197–251, Pergamon, Oxford.

CORDIER, P. and DOUKHAN, J.C. (1989): Water solubility in quartz and its influence on ductility. *Eur. J. Mineral.*, **1**, p. 221–237.

FLÖRKE, O.W., KÖHLER-HERBERTZ, B., LANGER, K. and TÖNGES, I. (1982): Water in microcrystalline quartz of volcanic origin: agates. *Contrib. Mineral. Petrol.*, **80**, p. 324–333.

FRONDEL, C. (1982): Structural hydroxyl in chalcedony (Type B quartz), *Am. Mineral.*, **67**, p. 1248–1257.

GRAETSCH, H., FLÖRKE, O.W. and MIEHE, G. (1985): The nature of water in chalcedony and opal-C from Brazilian agate geodes. *Phys. Chem. Miner*, **12**, p. 300–306.

GRAETSCH, H., FLÖRKE, O.H. and MIEHE, G. (1987): Structural defects in microcrystalline silica. *Phys. Chem. Miner*, **14**, p. 249–257.

GRIGGS, D. (1967): Hydrolytic weakening of quartz and other silicates. *Geophys. J. R. Astron. Soc.*, **14**, p. 19–31.

HARA, I. (1962): Studies of the structure of the Ryoke metamorphic rocks of the Kasagi district, southwest Japan. *J. Sci. Hiroshima Univ. Ser.* **C4**, p. 163–224.

HORDON, M.J. and AVERBACH, B.L. (1961): X-ray measurements of dislocation density in deformed copper and aluminum single crystals. *Acta Metall.*, **9**, p. 237–246.

KINGERY, W.D. (1960): *Introduction to ceramics.* Wiley, New York.

KLUG, H.P. and ALEXANDER, L.E. (1954): *X-ray diffraction procedures for polycrystalline and amorphous materials.* Wiley, New York.

LEVIEN, L., PREWITT, C.T. and WEIDNER, D.J. (1980): Structure and elastic properties of quartz at pressure, *Am. Mineral.*, **65**, p. 920–930.

MAYS, C.W., VERMAAK, J.S. and KUHLMANN-WILSDORF, D. (1968): On surface stress and surface tension II. Determination of the surface stress of gold. *Surf. Sci.*, **12**, p. 134–140.

MCLAREN, A.C., COOK, R.F., HYDE, S.T. and TOBIN, R.C. (1983): The mechanisms of the formation and growth of water bubbles and associated dislocation loop in synthetic quartz. *Phys. Chem. Miner*, **9**, p. 79–94.

MIEHE, G., GRAETSCH, H. and FLÖRKE, O.W. (1984): Crystal structure and growth fabric of length-fast chalcedony. *Phys. Chem. Miner*, **10**, p. 197–199.

MIYASHIRO, A. (1961): Evolution of metamorphic belts. *J. Petrol.*, **2**, p. 277–311.

MURATA, K.J. and NORMAN II, M.B. (1976): An index of crystallinity for quartz, *Am. J. Sci.*, **276**, p. 1120–1130.

NAGAHARA, M. (1969): Geology and ore deposits of the Ohtani mine, Kyoto Prefecture. *Suiyokaishi*, **16**, p. 697–700. (in Japanese)

NAGAO, H. and AIKAWA, N. (1985): Strain and size analyses from X-ray line broadening of pulverized quartz, *J. Geoscie., Osaka City Univ.*, **28**, p. 105–123.

NAGAO, H. and AIKAWA, N. (1988): Microstrain and crystallite size of natural microcrystalline quartz by X-ray line broadening analysis. *J. Am. Ceram. Soc.*, **71**, p. C421–C423.

NAKAJIMA, W. (1960): Geology of the northern margin of the Ryoke zone in the Yamato plateau. *Chikyu Kagaku (Earth Science)*, No. 49, p. 1–14. (in Japanese with English abstract)

NICHOLAS, A. and POIERIE, J.D. (1976): *Crystalline plasticity and solid state flow in metamorphic rocks.* Wiley, New York.

PARKS, G.A. (1984): Surface and interfacial free energy of quartz, *J. Geophys. Res.*, **89** [B6], p. 3997–4008.

SCHOENING, F.R.L. (1965): Strain and particle size values from X-ray line breadths, *Acta Crystallogr.*, **18**, p. 975–976.

SHIBATA, K. and MIZUTANI, S. (1982): Isotopic ages of Jurassic siliceous shale and Triassic bedded chert in Unuma, central Japan, *Geochem. J.*, **16**, p. 213–223.

VERMAAK, J.S., MAYS, C.W. and KUHLMANN-WILSDORF, D. (1968): On surface stress and surface tension I. Theoretical considerations. *Surf. Sci.*, **12**, p. 128–133.

VERMAAK, J.S. and KUHLMANN-WILSDORF, D. (1968): Measurement of the average surface stress of gold as a function of temperature in the temperature range 50–985°C. *J. Phys. Chem.*, **72**, p. 4150–4154.

VOOK, R.W. and OTOONI, M.A. (1968): Lattice parameter of thin gold films, *J. Appl. Phys.*, **39**, p. 2471–2472.

WASSERMAN, H.J. and VERMAAK, J.S. (1970): On the determination of a lattice contraction in very small silver particles. *Surf. Sci.*, **22**, p. 164–172.

WAN, G., BANNO, S. and TAKEUCHI, K. (1986): Reaction to define the biotite isograd in the Ryoke Metamorphic belt, Kii Peninnsula, Japan. *Contri. Mineral. Petrol.*, **93**, p. 9–17.

WARREN, B.E. (1959): X-ray studies of deformed metals. In CHALMERS, B. and KING, R. (eds.) *Progress in Metal Physics*, **8**, p. 147–202.

Explanation of Plate 1

Fig. 1 Bright-field electron micrograph of hardly metamorphosed chert (UN01). Magnification: ×150,000.

Fig. 2–3 Bright-field electron micrographs of metachert in the Kameoka district (KA21). Magnification: ×38,000.

Fig. 4 Bright-field electron micrograph of metachert in the Kameoka district (KA15). Magnification: ×75,000.


1

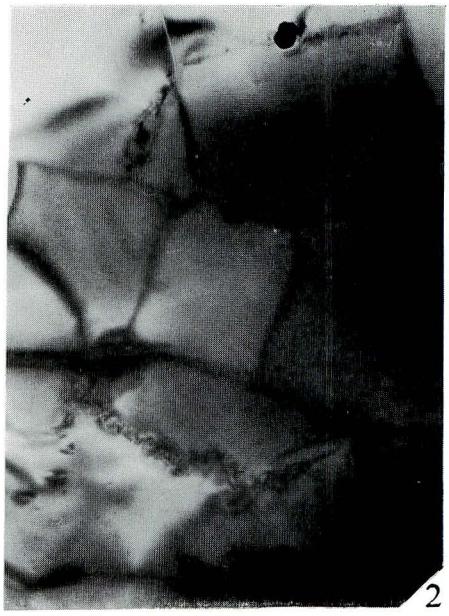
2

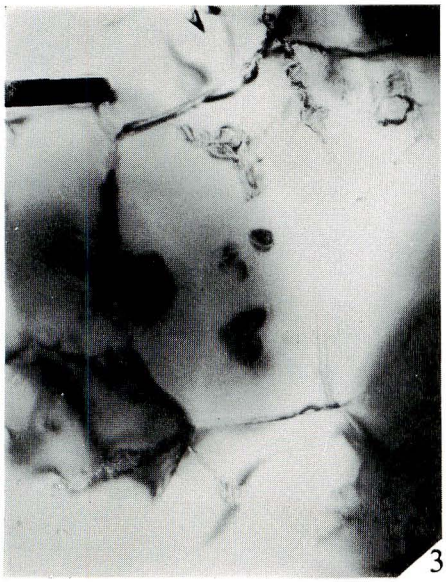
3


4

Explanation of Plate 2

Fig. 1–3 Bright-field electron micrographs of metachert in the Uji-Kasagi district (UK-41). Magnification: ×38,000 (Fig. 1–2), ×14,000 (Fig. 3).

Fig. 4 Bright-field electron micrograph of metachert in the Uji-Kasagi district (UK-128). Magnification: ×60,000.


1


2

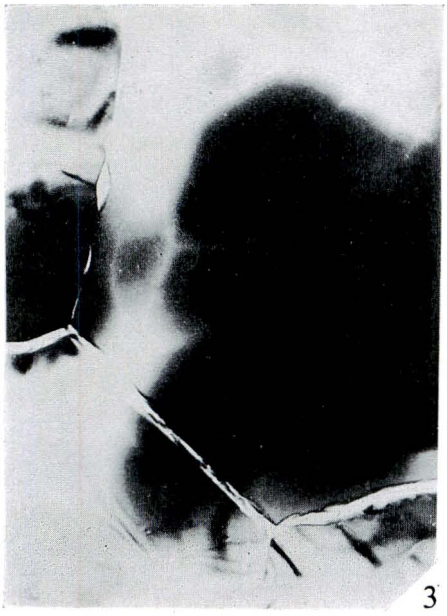
3

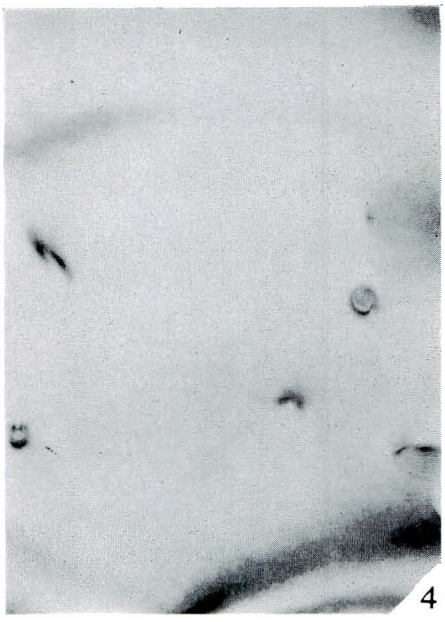
4